Article

Developmental Cell

Analysis of developmental imprinting dynamics in primates using SNP-free methods to identify imprinting defects in cloned placenta

Graphical abstract

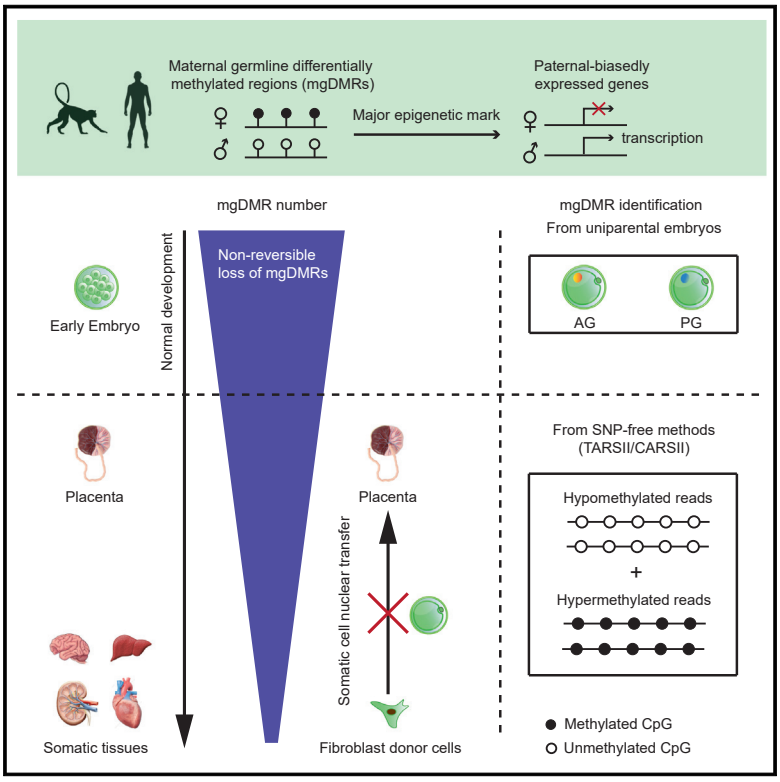

Highlights

- Maternal H3K27me3 is not a major mark for paternally expressed genes in monkey embryos
- Developing SNP-free methods that identify germline DMRs in outbred animals
- Primate germline DMRs are more highly enriched in placenta than in somatic tissues
- Placenta-specific germline DMRs are largely lost in monkey SCNT placenta

Authors

Chu Chu, Wenhao Zhang, Yu Kang, Chenyang Si, Weizhi Ji, Yuyu Niu, Yi Zhang

Correspondence

wenhao.zhang@childrens.harvard.edu (W.Z.),
wji@lpbr.cn (W.J.),
niuyy@lpbr.cn (Y.N.),
yzhang@genetics.med.harvard.edu (Y.Z.)

In brief

Chu and Zhang et al. develop SNP-free methods to identify germline differentially methylated regions (DMRs) in outbred animals. Germline DMRs in primate early embryos are largely lost during development and are biasedly maintained in placenta. This loss is non-reversible by SCNT, resulting in severe imprinting defects in cloned monkey placenta.

Chu et al., 2021, Developmental Cell *56*, 1–15
October 25, 2021
https://doi.org/10.1016/j.devcel.2021.09.012

CellPress

Developmental Cell

CellPress

Article

Analysis of developmental imprinting dynamics in primates using SNP-free methods to identify imprinting defects in cloned placenta

Chu Chu,[1,2,3,9] Wenhao Zhang,[4,5,6,9,*] Yu Kang,[1,2,3] Chenyang Si,[1,2,3] Weizhi Ji,[1,2,*] Yuyu Niu,[1,2,3,*] and Yi Zhang[4,5,6,7,8,10,*]

[1]State Key Laboratory of Primate Biomedical Research, Institute of Primate Translational Medicine, Kunming University of Science and Technology, Kunming, Yunnan 650500, China
[2]Yunnan Key Laboratory of Primate Biomedical Research, Kunming, Yunnan 650500, China
[3]Faculty of Life Science and Technology, Kunming University of Science and Technology, Kunming, Yunnan 650500, China
[4]Howard Hughes Medical Institute, Boston Children's Hospital, Boston, MA 02115, USA
[5]Program in Cellular and Molecular Medicine, Boston Children's Hospital, Boston, MA 02115, USA
[6]Division of Hematology/Oncology, Department of Pediatrics, Boston Children's Hospital, Boston, MA 02115, USA
[7]Department of Genetics, Harvard Medical School, Boston, MA 02115, USA
[8]Harvard Stem Cell Institute, WAB-149G, 200 Longwood Avenue, Boston, MA 02115, USA
[9]These authors contributed equally
[10]Lead contact
*Correspondence: wenhao.zhang@childrens.harvard.edu (W.Z.), wji@lpbr.cn (W.J.), niuyy@lpbr.cn (Y.N.), yzhang@genetics.med.harvard.edu (Y.Z.)
https://doi.org/10.1016/j.devcel.2021.09.012

SUMMARY

Our knowledge of genomic imprinting in primates is lagging behind that of mice largely because of the difficulties of allelic analyses in outbred animals. To understand imprinting dynamics in primates, we profiled transcriptomes, DNA methylomes, and H3K27me3 in uniparental monkey embryos. We further developed single-nucleotide-polymorphism (SNP)-free methods, TARSII and CARSII, to identify germline differentially methylated regions (DMRs) in somatic tissues. Our comprehensive analyses showed that allelic DNA methylation, but not H3K27me3, is a major mark that correlates with paternal-biasedly expressed genes (PEGs) in uniparental monkey embryos. Interestingly, primate germline DMRs are different from PEG-associated DMRs in early embryos and are enriched in placenta. Strikingly, most placenta-specific germline DMRs are lost in placenta of cloned monkeys. Collectively, our study establishes SNP-free germline DMR identification methods, defines developmental imprinting dynamics in primates, and demonstrates imprinting defects in cloned monkey placenta, which provides important clues for improving primate cloning.

INTRODUCTION

Genomic imprinting is an allelic gene expression phenomenon that plays critical roles in multiple biological processes including development, behavior, brain functions, circadian clock, and diseases (Barlow and Bartolomei, 2014; Peters, 2014; Tucci et al., 2019). Despite the intensive studies on genomic imprinting in the last decades, our knowledge of genomic imprinting, especially in outbred animals such as primates, is still limited.

DNA methylation has long been considered as the only primary imprinting mark in mammals until recently when we discovered that maternal-biased H3K27me3 can also mediate dozens of paternal-biasedly expressed genes (PEGs) in mouse preimplantation embryos (Chen et al., 2019; Chen and Zhang, 2020; Inoue et al., 2017). However, whether this imprinting mechanism is conserved in primates remains to be resolved (Xia et al., 2019; Zhang et al., 2019).

On the other hand, our knowledge on genomic imprinting dynamics during primate embryonic development is also limited. For example, although recent studies have identified allelically expressed genes and allelic differentially methylated regions (DMRs) in human early embryos (Sagi et al., 2019; Zhu et al., 2018), whether these allelically expressed genes and their associated DMRs identified in early embryos are maintained in somatic tissues is not clear. Furthermore, although some of the placenta-specific imprinted genes have been reported in humans (Court et al., 2014; Hamada et al., 2016; Hanna et al., 2016; Sanchez-Delgado et al., 2016), it is not clear whether more placenta-specific imprinted genes exist and whether such placenta-specific imprinting is conserved among primates.

One of the major reasons that limited our understanding of genomic imprinting in outbred animals, such as primates, is the lack of efficient methods to distinguish parental alleles. Currently, *de novo* identification of genome-wide allelic DMRs in human

Please cite this article in press as: Chu et al., Analysis of developmental imprinting dynamics in primates using SNP-free methods to identify imprinting defects in cloned placenta, Developmental Cell (2021), https://doi.org/10.1016/j.devcel.2021.09.012

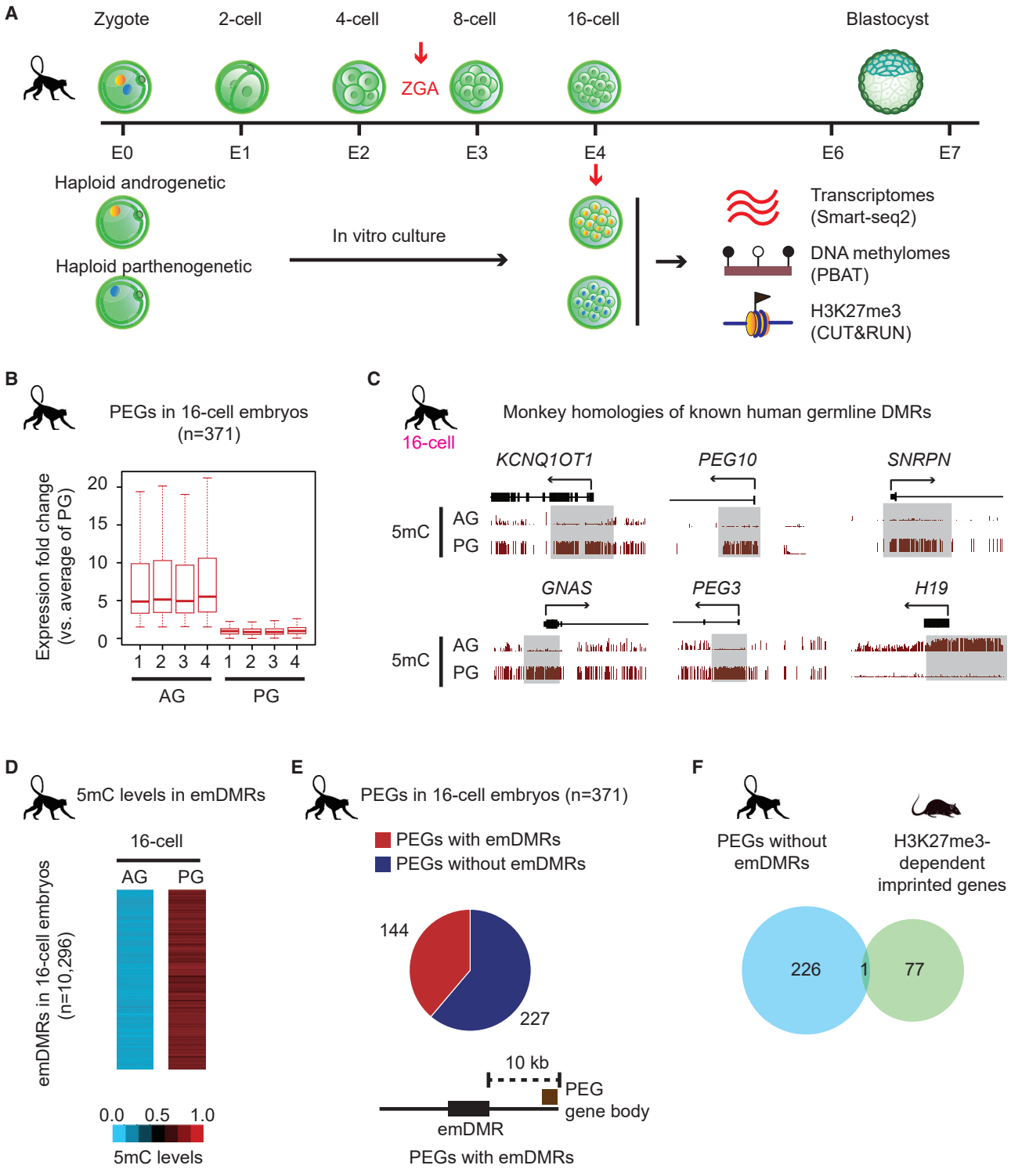

Figure 1. Identification of DNA-methylation-associated and DNA-methylation-unassociated embryonic PEGs

(A) A schematic diagram of the experimental designs for this study.

(B) Boxplots showing fold changes of PEGs in uniparental monkey embryos. The fold change for a particular gene in each sample is calculated using the gene expression level (fragments per kilobase per million, FPKM) of that sample divided by the average expression level (FPKM) of all samples of PG embryos.

(C) UCSC genome browser snapshots showing parental 5mC levels in monkey AG and PG embryos for monkey homologies of known germline DMRs in humans.

(D) A heatmap showing 5mC levels of emDMRs in 16-cell AG and PG monkey embryos.

(legend continued on next page)

Please cite this article in press as: Chu et al., Analysis of developmental imprinting dynamics in primates using SNP-free methods to identify imprinting defects in cloned placenta, Developmental Cell (2021), https://doi.org/10.1016/j.devcel.2021.09.012

somatic tissues requires integrating hundreds of methylomes from different individuals using single-nucleotide polymorphism (SNP)-based analyses (Zink et al., 2018) or applying special samples such as those with uniparental disomy (Joshi et al., 2016). These methods are expensive and impractical to be widely used in the studies of genomic imprinting in outbred animals.

In this study, by profiling transcriptomes, DNA methylomes, and H3K27me3 in uniparental monkey embryos, we show that allelic DNA methylation, but not H3K27me3, majorly correlates with PEGs in monkey early embryos. In addition, we have developed SNP-free methods that allow robust and accurate identification of germline DMRs in somatic tissues in outbred animals. Using these methods, we revealed genomic imprinting differences in primates between early embryos and somatic tissues, as well as between embryonic and extraembryonic tissues. Importantly, based on the developmental imprinting dynamics in primates, we hypothesized and demonstrated that cloned monkey placenta exhibits severe imprinting defects, which provides important clues for improving primate cloning.

RESULTS

DNA-methylation-associated PEGs in monkey early embryos

To better understand regulation mechanisms of genomic imprinting in primates, we profiled transcriptomes, DNA methylomes, and H3K27me3 in monkey (*Macaca fascicularis*) haploid androgenetic (AG) and parthenogenetic (PG) 16-cell embryos (Figures 1A and S1A; Table S1). The high correlation between the transcriptome replicates of AG and PG embryos confirmed the data quality (Figure S1B). To confirm that proper zygotic genome activation (ZGA) was achieved in the uniparental embryos, we first identified 2,084 ZGA genes by comparing transcriptomes of 4-cell (pre-ZGA) and 8-cell (ZGA) monkey embryos using a public dataset (Liu et al., 2018) (Table S2) and then analyzed the expression levels of these ZGA genes in the uniparental embryos. This analysis showed that the expression levels of the ZGA genes in the uniparental embryos are similar to that in the 8-cell embryos but are significantly higher than those in the 4-cell embryos (Figure S1C), indicating that ZGA has taken place normally in the uniparental embryos.

Previous studies have indicated that the majority of the germline DMRs harbor maternal-specific DNA methylation in somatic tissues of mice and humans, resulting in paternal-biased expression (Babak et al., 2015; Court et al., 2014; Xie et al., 2012). In addition, the H3K27me3-dependent imprinted genes in mouse early embryos and placenta also exhibit paternal-biased expression, due to the oocyte-inherited maternal-specific H3K27me3 (Inoue et al., 2017). Thus, to understand the developmental dynamics of imprinting, we choose to focus on PEGs. Using relatively stringent criteria (AG (FPKM) $\geq$ 2, AG/PG (FPKM) $\geq$ 3, each AG replicate/PG (FPKM) $\geq$ 1.5) and excluding genes on the sex chromosomes, we identified a total of 371 PEGs in monkey 16-cell embryos (Figure 1B; Table S2).

To identify the early-embryonic maternal-allele-methylated differentially methylated regions (emDMRs) associated with the 371 PEGs in monkeys, we profiled DNA methylomes of AG and PG 16-cell embryos in monkeys by post-bisulfite adaptor tagging (PBAT) (Miura et al., 2012) (Figure 1A). To exam whether allelic DNA methylation can be faithfully captured in uniparental embryos, we analyzed DNA methylation of uniparental embryos at the genomic regions corresponding to the known human germline DMRs (Court et al., 2014). We found that all the corresponding genomic regions exhibit the same maternal-biased or paternal-biased DNA methylation in uniparental monkey embryos as those in humans (see Figure 1C for examples), demonstrating that the allelic DNA methylation is faithfully maintained in the uniparental embryos.

To determine which of the 371 PEGs in early embryos are likely regulated by the emDMRs, we compared the DNA methylation profiles of AG and PG 16-cell monkey embryos and identified 10,296 emDMRs (AG 5mC $\geq$ 0.15, PG-AG 5mC $\geq$ 0.5) (Figure 1D; Table S2). Using a cutoff of 10 kilobase (kb) from emDMR to gene body, we identified 144 PEGs that are closely associated with the emDMRs (Figure 1E; Table S2). Interestingly, the remaining 227 PEGs without emDMRs (within 10 kb) showed little overlap with the homologies of the 78 putative H3K27me3-dependent imprinted genes in mice (Figures 1E and 1F) (Chen et al., 2019; Inoue et al., 2017), indicating that the H3K27me3-dependent imprinted genes in mice may not be conserved in monkeys.

H3K27me3 is not a major mark for PEGs in monkey early embryos

To directly examine whether maternal-biased H3K27me3 correlates with PEGs in monkey early embryos similar to that in mice, we profiled H3K27me3 by cleavage under targets and release using nuclease (CUT&RUN) (Skene and Henikoff, 2017) in uniparental 16-cell monkey embryos (Figure 1A). Consistent with a repressive role of H3K27me3 in transcription (Cao et al., 2002), a clear anti-correlation between gene expression and gene body H3K27me3 levels were observed (Figure S2A), validating the H3K27me3 profiles. Interestingly, an initial inspection revealed a similar H3K27me3 distribution pattern in both AG and PG 16-cell embryos in monkeys, which contrasts with the maternal-biased H3K27me3 enrichment in mice at a similar stage (Figure 2A) (Zheng et al., 2016). This observation is further confirmed by both chromosome-wide and genome-wide comparisons (Figures 2B and 2C), indicating that H3K27me3 is largely distributed bi-allelically in monkey 16-cell embryos.

Since a recent study showed that global loss of H3K27me3 takes place at 8-cell stage in human embryos (Xia et al., 2019), it is possible that a similar global loss of H3K27me3 at 8-cell stage may also occur in monkeys. To test this possibility, we performed immunofluorescent staining of H3K27me3 at different stages of monkey preimplantation embryos and found that H3K27me3 signal decreases from zygote to 8-cell embryos and increases from 8-cell embryo to blastocyst (Figures 2D and 2E). To further demonstrate that H3K27me3 reprograming

(E) A pie chart showing the number of PEGs with/without emDMRs in 10-kb distance from their gene bodies.
(F) A Venn diagram showing overlap between PEGs without emDMR identified in monkey early embryos and the H3K27me3-dependent imprinted genes identified in mouse early embryos (Chen et al., 2019; Inoue et al., 2017).
See also Figure S1 and Tables S1 and S2.

Please cite this article in press as: Chu et al., Analysis of developmental imprinting dynamics in primates using SNP-free methods to identify imprinting defects in cloned placenta, Developmental Cell (2021), https://doi.org/10.1016/j.devcel.2021.09.012

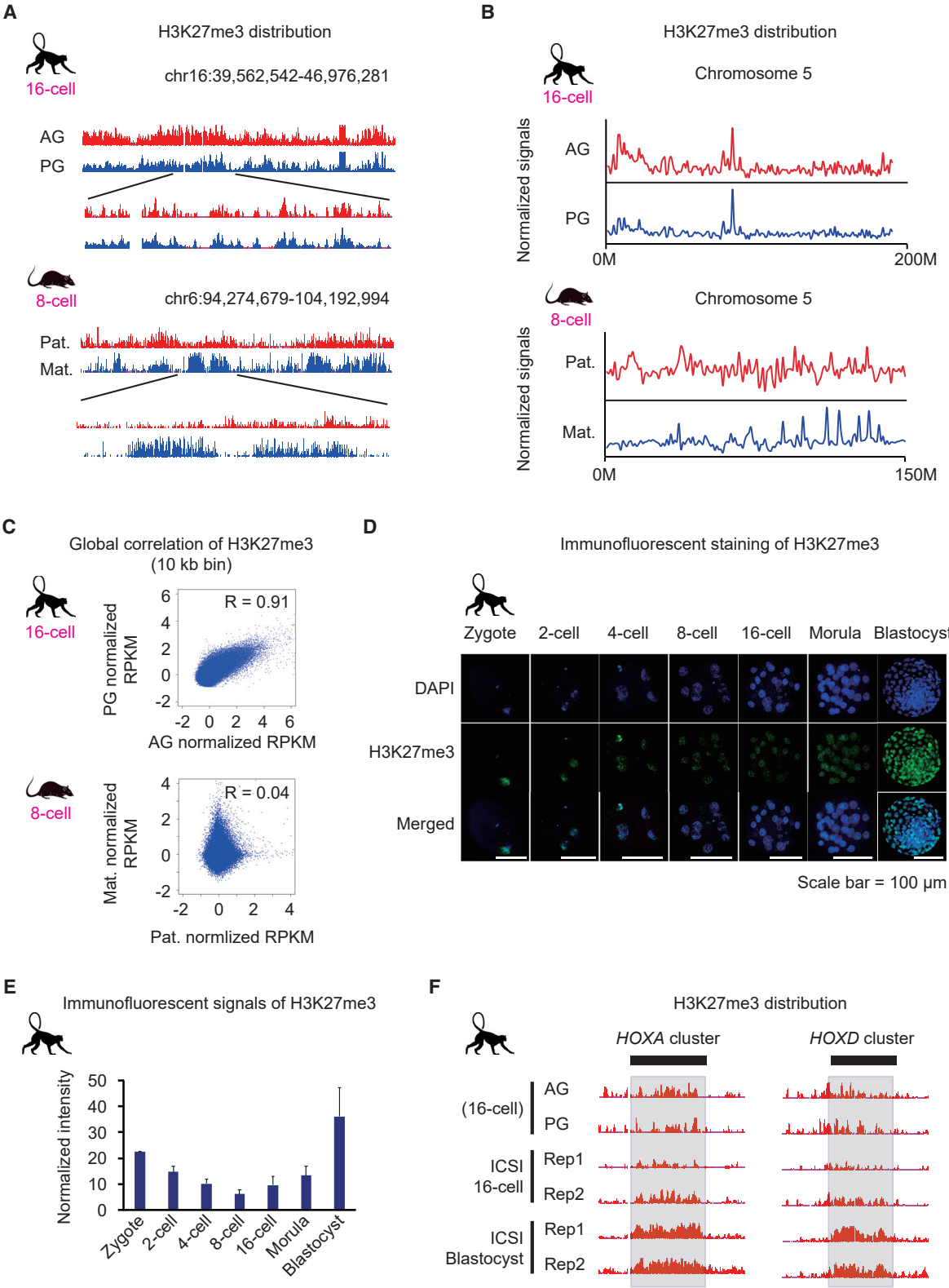

Figure 2. H3K27me3 is globally reprogrammed in monkey early embryos

(A–C) A comparison of H3K27me3 distribution in uniparental 16-cell monkey embryos (upper panel), as well as H3K27me3 distribution in paternal and maternal alleles of 8-cell mouse embryos (bottom panel), by UCSC genome browser snapshots (A), chromosome-wide line graph (B), and genome-wide scatterplots (in 10-kb bin, Pearson correlation coefficient calculated) (C).

(legend continued on next page)

Please cite this article in press as: Chu et al., Analysis of developmental imprinting dynamics in primates using SNP-free methods to identify imprinting defects in cloned placenta, Developmental Cell (2021), https://doi.org/10.1016/j.devcel.2021.09.012

indeed occurs in monkey early embryos, we profiled H3K27me3 by CUT&RUN in monkey 16-cell embryos and blastocysts generated by intracytoplasmic sperm injection (ICSI). The high correlations of H3K27me3 signals between the replicates of 16-cell embryos and blastocysts, as well as between 16-cell embryos of AG/PG and ICSI (Figure S2B), again validated the good quality of our H3K27me3 dataset. As expected, the enrichment of H3K27me3 on developmental genes such as *HOX* clusters, *PAX6*, *SOX14*, *NEUROD2*, and *FOXL2* are clearly increased from 16-cell embryos to blastocysts (Figures 2F and S2C), indicating that reprogramming of H3K27me3 takes place during monkey preimplantation development. In contrast, establishment of H3K27me3 on typical developmental genes in mice mainly takes place during post-implantation development (Zheng et al., 2016).

Consistent with the observed H3K27me3 dynamics, we found that *EED* and *SUZ12*, two core components of polycomb repressive complex 2 (PRC2) responsible for H3K27me3 deposition (Cao et al., 2002) are barely detectable in 4-cell monkey embryos preceding ZGA (Figure S2D), indicating that global H3K27me3 cannot be maintained in monkey embryos before ZGA. In contrast, all three PRC2 core components are highly expressed in mouse embryos preceding ZGA (Figure S2D).

Notably, despite H3K27me3 being globally similar between AG and PG uniparental monkey embryos and likely reprogrammed during ZGA, which is clearly different from the observation in mice (Figures 2A–2C), we cannot rule out the possibility that certain regions could have maternal-biased H3K27me3, which may regulate PEGs. To explore the general relationship between maternal-biased H3K27me3 and PEGs in monkey early embryos, we first identified 681 PG-biased H3K27me3 regions across the genome (Figure S2E; Table S2). Then, using a cutoff of 10-kb distance, we found that 7 out of the 227 PEGs without an emDMR are related to PG-biased H3K27me3 (Figures 1E and S2F). Collectively, the above results suggest that, in contrast to mice, H3K27me3 in monkeys is globally reprogrammed and unlikely to be a major mark regulating PEG expression in monkey preimplantation embryos.

Identification of putative imprinted DMRs by TARSII using somatic tissue methylomes

The above analyses indicate that maternal-specific DNA methylation, but not H3K27me3, is a major regulator of PEGs in monkey early embryos. To determine whether the PEG-associated emDMRs (PEG-emDMRs) presented in early embryos are maintained in somatic tissues, identification of maternal germline DMRs in monkey somatic tissues is required. However, since no inbred monkey strains are available, *de novo* identification of germline DMRs in monkey somatic tissues would require large number of materials and datasets to assign allelic methylation through SNPs.

Thus, we attempted to overcome this technical barrier by developing a method named TARSII (tissue-associated, reads-based, SNP-free method for identifying imprint-DMRs) that allows identification of genome-wide germline DMRs without annotating SNPs. To this end, genomic regions with at least 10 consecutive partially methylated CpGs (5-mC level: 0.3–0.7) are first identified as partially methylated domains (PMDs) (Figure 3A, left panel). Then, to fulfill the allele-specific methylation event, the identified PMDs are required to enrich for both hypomethylated reads (CpG number $\geq$ 3, 5mC $\leq$ 0.2) and hypermethylated reads (CpG number $\geq$ 3, 5mC $\geq$ 0.8) (Figure 3A, middle panel). To determine the proper percentages of hypomethylated and hypermethylated reads versus total reads on germline DMRs, we analyzed the methylation states of previously known mouse germline DMRs using a deeply sequenced methylome (Xie et al., 2012). We found that most of the known germline DMRs have a minimal 30% of both hypomethylated and hypermethylated reads (Figure S3A). Since most germline DMRs are consistently imprinted across different tissues, we integrated six different mouse tissues (cortex, cerebellum, heart, intestine, kidney, and liver) derived from three germ layers (two tissues from each germ layer) to increase the accuracy (Figure 3A, right panel). This analysis identified a total of 6,208 candidate DMRs from the methylomes of the six mouse tissues (Figure S3B). As expected, the candidate DMRs commonly identified in those tissues decrease as the number of tissues required increases (Figure S3B). In contrast, the prediction accuracy (overlapping between candidate DMRs and the known imprinted DMRs) is significantly increased and reached a peak of 91.7% when a minimum of 5 tissues is required (Figure S3C). Consequently, we applied a cutoff of 5 as the minimal number of tissues required for identifying putative imprinted DMR by TARSII (Figure 3A, right panel). We also tested different cutoffs for the number of minimal reads in each candidate DMR and found a minimal of 30 reads produced the best result (Figure S3D). When these cutoffs are used in TARSII, we identified 24 putative imprinted DMRs based on the mouse somatic tissue methylomes without using SNP information (Table S3).

Validation of TARSII-identified germline DMRs in mice and humans

Since TARSII is majorly designed to identify germline DMRs that are consistent in different somatic tissues, we next tested the accuracy and efficiency of TARSII in predicting germline DMRs in mice. By comparing the mouse sperm and oocyte methylomes, we identified 17 putative maternal germline DMRs (mgDMRs) and 3 putative paternal germline DMRs (pgDMRs) from the 24 TARSII predicted imprinted DMRs (Figures 3B and S3E; Table S3). Interestingly, all the 17 TARSII predicted mgDMRs overlap with the known mgDMRs in mice (Figure 3C; Table S3) and the 3 TARSII predicted pgDMRs (*Rasgrf1*, *Gpr1*, and *H19*) also overlap with the known pgDMRs (Table S3) (Kikyo et al., 1997; Xie et al., 2012), indicating a 100% accuracy of prediction for mouse germline DMRs.

(D) Immunofluorescent staining of H3K27me3 in monkey preimplantation embryos at different stages.
(E) Quantification of the immunofluorescent signals of H3K27me3 in Figure 2D. Data are represented as mean ± SEM.
(F) UCSC genome browser snapshots showing H3K27me3 enrichment at HOXA and HOXD clusters in monkey AG and PG 16-cell embryos, as well as in 16-cell embryos and blastocysts derived by intracytoplasmic sperm injection (ICSI) in monkey.
See also Figure S2 and Tables S1 and S2.

Please cite this article in press as: Chu et al., Analysis of developmental imprinting dynamics in primates using SNP-free methods to identify imprinting defects in cloned placenta, Developmental Cell (2021), https://doi.org/10.1016/j.devcel.2021.09.012

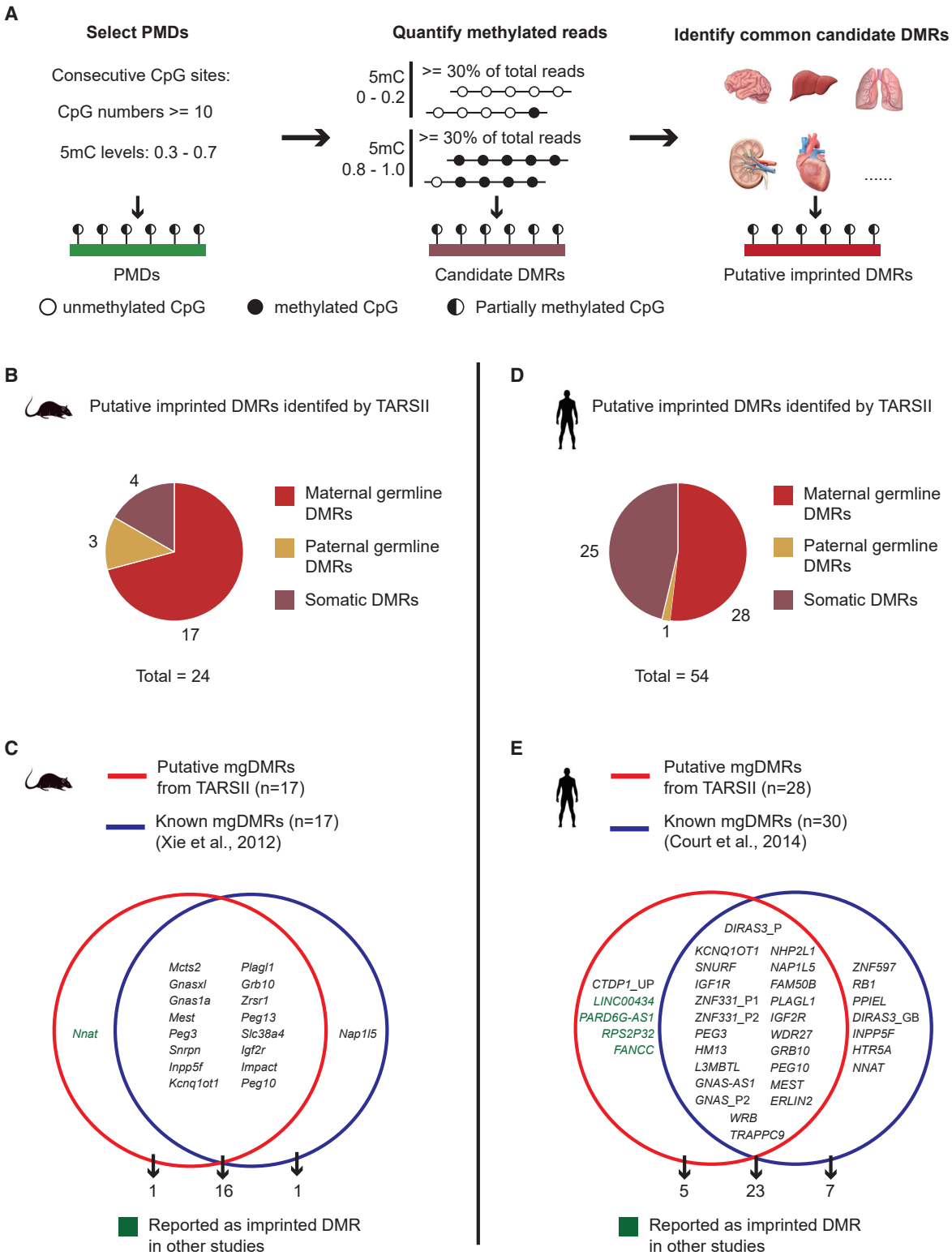

Figure 3. Identification of putative germline DMRs by TARSII

(A) A schematic presentation of TARSII. Briefly, regions contain over 10 consecutive CpGs with 5 mC levels ranging from 0.3 to 0.7 were selected as PMDs (left panel). PMDs enriched for both hypomethylated reads (5mC $\leq$ 0.2) and hypermethylated reads (5mC $\geq$ 0.8) are considered as candidates (middle panel). Finally, candidates commonly identified in at least 5 different tissues are selected as putative imprinted DMRs (right panel).

(B) A pie chart showing the different categories of putative imprinted DMRs in mice based on 5 mC levels in oocyte and sperm.

(legend continued on next page)

Please cite this article in press as: Chu et al., Analysis of developmental imprinting dynamics in primates using SNP-free methods to identify imprinting defects in cloned placenta, Developmental Cell (2021), https://doi.org/10.1016/j.devcel.2021.09.012

Having demonstrated the accuracy and efficiency of TARSII in identifying mouse germline DMRs, next, we tested its predictability in humans by applying TARSII to publicly available human methylomes from six different tissues (brain, muscle, aorta, lung, liver, and intestine) (Table S1). This analysis identified 54 putative imprinted DMRs (Figures 3D and S3F; Table S3). To distinguish mgDMRs from that of pgDMRs and somatic DMRs, we combined the above analysis with the AG and PG methylomes in human 8-cell embryos from a public dataset (Leng et al., 2019). This integrative analysis allowed us to identify 28 putative mgDMRs and 1 putative pgDMR in humans (Figure 3D; Table S3). Importantly, 23 out of the 28 putative mgDMRs overlap with the 30 known mgDMRs (Figure 3E; Table S3), and the 1 putative pgDMR (*H19*) also overlaps with the 2 known pgDMRs (IG-DMR, *H19*) (Table S3) in humans compiled in a previous study (Court et al., 2014). Notably, 4 out of the 5 remaining putative mgDMRs have been validated in several recent studies (de Sa Machado et al., 2018; Grothaus et al., 2016; Jadhav et al., 2019; Joshi et al., 2016; Sanchez-Delgado et al., 2016) (Figure 3E). Thus 27 out of the 28 (96.4%) putative mgDMRs identified by TARSII overlap with the known mgDMRs in humans (Figure 3E). Taken together, the above results support the efficiency and accuracy of TARSII in identifying genome-wide germline DMRs from somatic tissue methylomes without SNP information.

Most PEG-emDMRs in early embryos are not maintained in somatic tissues

Having validated the predictability of TARSII for germline DMRs in both mice and humans based on their somatic tissue methylomes, next, we applied it to monkeys. To this end, we profiled methylomes of six different tissues (cerebellum, cortex, heart, kidney, liver, and intestine) of an adult monkey. By analyzing these methylomes using TARSII, we identified 63 putative imprinted DMRs in monkeys (Figure S4A; Table S3). When combined with the analysis of the 16-cell AG and PG methylomes in monkeys (Figures 1A and 1D), we identified 39 putative mgDMRs in monkeys (Figure S4A; Table S3). We found previously reported monkey imprinted DMRs (*IGF2R*, *INPP5F*, *KCNQ1OT1*, *NAP1L5*, *PEG3*, *SNURF*, and *PAGL1*) are all detected by TARSII (Figure 4A) (Cheong et al., 2015; Wianny et al., 2016). Interestingly, 27 (including *RPS2P32*) out of the 39 putative mgDMRs are counterparts of the known mgDMRs in humans (Court et al., 2014; Grothaus et al., 2016) (Figure 4A; Table S3), indicating the conservation of mgDMRs between humans and monkeys. To validate the remaining 12 putative mgDMRs in monkeys, we analyzed the allelic DNA methylation based on SNPs using CGmapTools, a method used to calculate allelic DNA methylation based on whole genome bisulfite sequencing dataset (Guo et al., 2018). We found that 10 out of the 12 putative mgDMRs have SNPs in our monkey methylomes, and 7 of them (*PLD6*, *GABRG3*, *C17orf97*, *VPS26C*, *ZNF557*, *TEX29,* and *PRMT2*) showed significant allelic methylation differences, supporting their imprinted state (Figure S4B). Therefore, of the 39 TARSII identified mgDMRs in monkeys, 27 are counterparts of the known mgDMRs in humans, and 7 of the 10 remaining mgDMRs with SNPs exhibit allelic DNA methylation, again validating the accuracy of TARSII in predicting germline DMRs. Using CGmapTools, we found the putative mgDMR for *CTDP1*_UP, which was identified by TARSII in humans, exhibits allelic DNA methylation, supporting its imprinted state (Figures 3E and S4C).

Next, we studied the imprinting dynamics between early embryos and somatic tissues in monkeys by comparing the PEG-emDMRs in early embryos and mgDMRs in somatic tissues. Using 10-kb distance from gene bodies of PEGs to the emDMRs (Figures 1B and 1D) as a cutoff to define an association, we identified 276 PEG-emDMRs in monkey (16 cell) early embryos (Figure 4B; Table S2). Surprisingly, when the PEG-emDMRs are compared with the TARSII identified mgDMRs in monkeys (Figure 4A), only 4 are overlapped (Figure 4B). This indicates PEGs are also largely different between early embryos and somatic tissues in monkeys. To determine whether this phenomenon is conserved in humans, we analyzed public transcriptome and methylome datasets in uniparental 8-cell embryos of humans (Leng et al., 2019). By applying the same methods and cutoffs used in our investigation of monkeys, we identified 271 PEGs and 24,501 emDMRs in human 8-cell embryos (Figures S4D and S4E), defining 334 PEG-emDMRs (Figure 4C; Table S2). Similar to monkeys, only 2 PEG-emDMRs in early embryos are overlapped with the 35 putative and known mgDMRs in somatic tissues in humans (Figures 3E and 4C), supporting that PEGs are different between early embryos and somatic tissues in primates. In contrast, the 35 mgDMRs are associated with 27 known PEGs identified in human somatic tissues (Babak et al., 2015) (Figure S4F).

The imprinting differences between early embryos and somatic tissues are likely caused by the global DNA methylation reprogramming during mammalian early embryonic development (Sanchez-Delgado et al., 2016; Smallwood et al., 2011). Although the large number of emDMRs appear to mediate paternal-biased expression in preimplantation embryos, most emDMRs are reprogrammed after implantation and lose their imprinted state in somatic tissues (Figures 4D and 4E, for example). Collectively, our analyses demonstrate that most PEG-emDMRs in primate early embryos are not maintained in somatic tissues, supporting differential imprinting between early embryos and somatic tissues of primates.

Identification of tissue-specific maternal germline DMRs by CARSII

As mentioned above, some placenta-specific imprinted genes regulated by placenta-specific mgDMRs have been identified in humans (Court et al., 2014; Hamada et al., 2016; Sanchez-Delgado et al., 2016), suggesting human placenta tend to maintain

(C) A Venn diagram showing the overlap between putative mgDMRs identified by TARSII in mice and the known mgDMRs summarized in a previous study (Xie et al., 2012) (Table S3).

(D) A pie chart showing the different categories of putative imprinted DMRs in human based on 5 mC levels in AG and PG 8-cell embryos.

(E) A Venn diagram showing overlap between putative mgDMRs identified by TARSII in human and the known mgDMRs summarized in a previous study (Court et al., 2014) (Table S3).

See also Figure S3 and Tables S1 and S3.

Please cite this article in press as: Chu et al., Analysis of developmental imprinting dynamics in primates using SNP-free methods to identify imprinting defects in cloned placenta, Developmental Cell (2021), https://doi.org/10.1016/j.devcel.2021.09.012

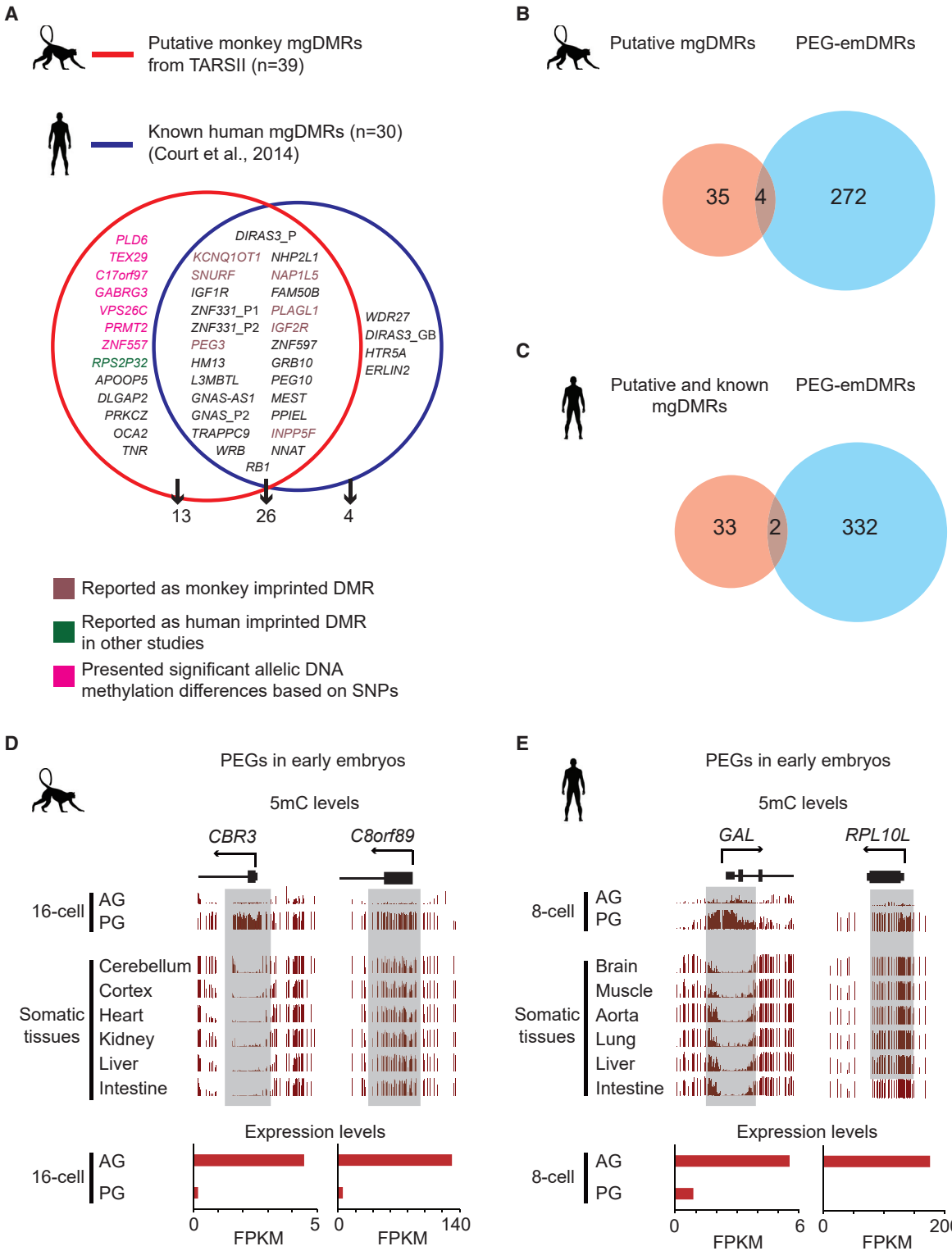

Figure 4. Most PEG-emDMRs are not maintained in somatic tissues of primates

(A) A Venn diagram showing overlap between putative mgDMRs identified by TARSII in monkeys and the known mgDMRs in humans summarized in a previous study (Court et al., 2014) (Table S3).

(B and C) Venn diagrams showing overlap between PEG-emDMRs in early embryos and the putative and known mgDMRs in monkeys (B) and humans (C).

(D and E) UCSC genome browser snapshots showing 5mC levels of representative PEG-emDMRs in early embryos and somatic tissues, as well as related PEG expression in early embryos of monkeys (D) and humans (E).

See also Figure S4 and Tables S1 and S3.

Please cite this article in press as: Chu et al., Analysis of developmental imprinting dynamics in primates using SNP-free methods to identify imprinting defects in cloned placenta, Developmental Cell (2021), https://doi.org/10.1016/j.devcel.2021.09.012

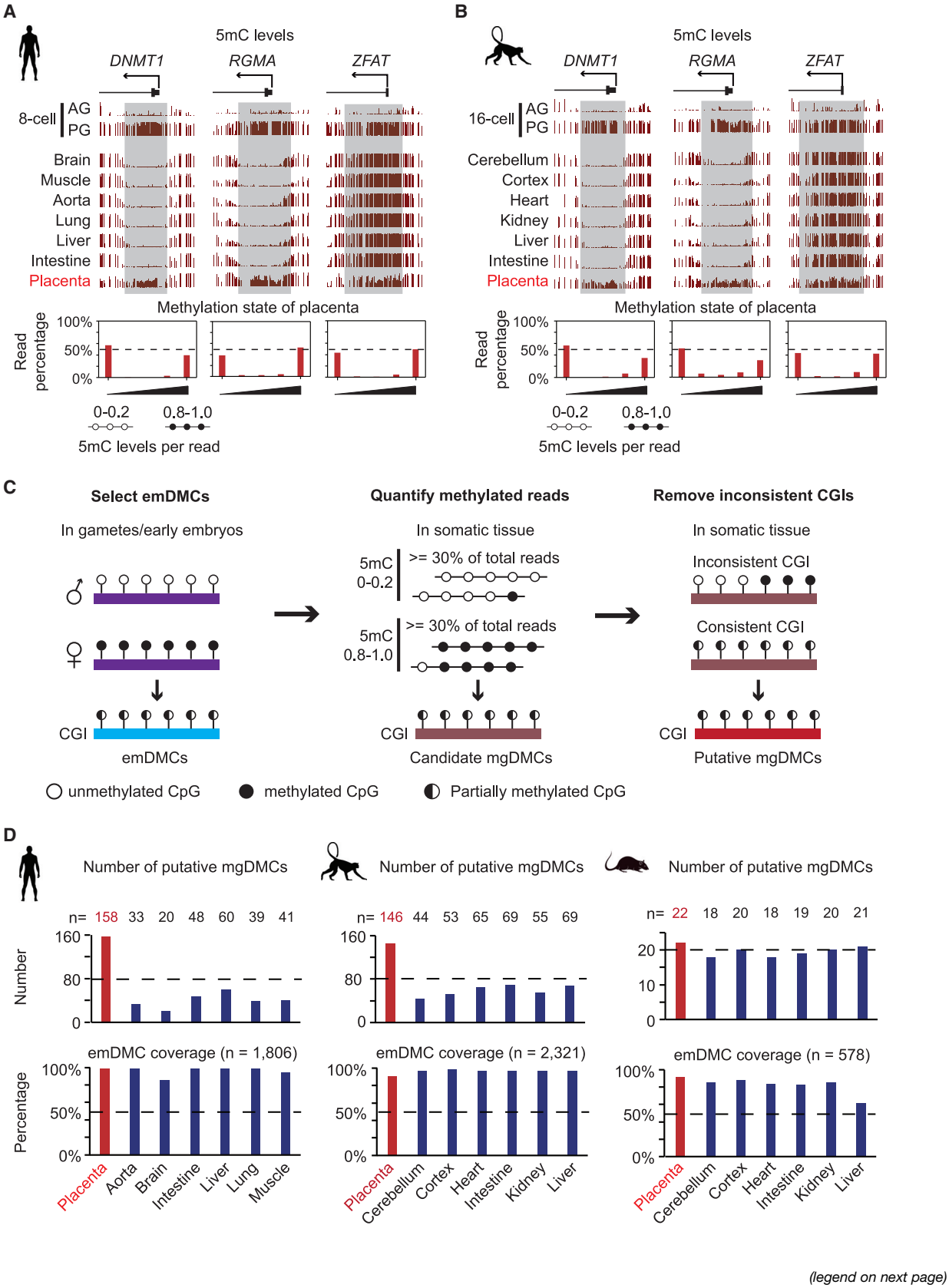

(legend on next page)

Please cite this article in press as: Chu et al., Analysis of developmental imprinting dynamics in primates using SNP-free methods to identify imprinting defects in cloned placenta, Developmental Cell (2021), https://doi.org/10.1016/j.devcel.2021.09.012

maternal-specific DNA methylation in early embryos. Interestingly, by profiling and analyzing placenta methylome in monkeys, we noticed that the monkey counterpart of human placenta-specific mgDMRs is also partially methylated in monkey placenta (Figures 5A and 5B, upper panels). Further analyses revealed those regions are enriched for both hypermethylated and hypomethylated reads in human and monkey placenta (Figures 5A and 5B, bottom panels), fulfilling a DNA methylation imprinted state.

To further investigate the maintenance of PEG-emDMRs in placenta and the placenta-specific imprinting in primates, we attempted to identify mgDMRs from a single tissue such as placenta. Since TARSII requires integration of methylomes from multiple tissues for accurate prediction, we developed another method named CARSII (CpG-island-associated, reads-based, SNP-free method for identifying imprint-DMRs) with the aim to predict germline DMRs in a tissue-specific manner (Figure 5C). To minimize the variation caused by tissue cell heterogeneity and facilitate comparison between different tissues, we have restricted the type of mgDMR candidates to early-embryonic maternal-allele-methylated differential methylated CpG-islands (emDMCs) identified from gametes or early embryos (Figure 5C, left panel; Figure S5A; Table S4). The reasons for focusing on emDMCs are as follows: first, CpG islands (CGIs) are usually important transcriptional regulatory elements, whose methylation level is subjected to tight regulation of multiple factors and is more stable compared with other regions in the genome (Deaton and Bird, 2011). Second, most mgDMRs overlap with emDMCs. For examples, 15 (88.2%) of the 17 known mgDMRs in mice (Xie et al., 2012) (Table S3) and 23 (76.7%) of the 30 known mgDMRs in humans (Court et al., 2014) (Table S3) overlap with their emDMCs (Figure S5B). In contrast, emDMCs only occupy ~0.01% of the mice and ~0.03% of the human genome (Figure S5A). This indicates that the chance to identify a mgDMR from emDMC is a thousand times higher than that from other regions of the genome. Thus, focusing on emDMCs can greatly increase the chance of predicting mgDMRs from a single tissue.

After selecting the emDMCs based on methylomes of gametes or early embryos (Figure S5A; Table S4), we further determined the enrichment of both hypermethylated and hypomethylated reads on these emDMCs in certain somatic tissue with algorithms similar to TARSII and removed the candidates with false positive rate (FPR) $\geq$ 0.05 (Figure 5C, middle panel). Although the majority of candidates harbored consistent partially methylated CpGs along the CGI, a few showed inconsistent methylation and were filtered out (Figure 5C, right panel). Then, the remaining mgDMR candidates were recognized as putative maternal germline differential methylated CpG islands (mgDMCs) in each tissue. To test the accuracy and efficiency of putative mgDMCs predicted by CARSII, we applied CARSII to mouse methylomes and identified 18–21 putative mgDMCs from several individual somatic tissues (Figure S5C; Table S5). ~70%–100% of these putative mgDMCs identified by CARSII overlap with the known mgDMRs in mice (Xie et al., 2012) (Figure S5C; Table S3). Considering the existence of tissue-specific mgDMRs, such as *Cdh15* and *Myo10* (Proudhon et al., 2012; Xie et al., 2012), the accuracy of CARSII could be even higher. Collectively, CARSII exhibited great accuracy in predicting mgDMCs (represent mgDMRs) in individual tissue.

Primate mgDMCs are more enriched in placenta than in somatic tissues

Next, we applied CARSII to human and monkey tissue methylomes and identified putative mgDMCs in both placenta and somatic tissues (Figure 5D; Table S5). Surprisingly, while an average of 40 mgDMCs were identified in human somatic tissues, similar analysis revealed 158 mgDMCs in placenta (Figure 5D, left up panel), indicating that the mgDMCs in humans are much more enriched in placenta than that in somatic tissues. Notably, the lower numbers of putative mgDMCs in somatic tissues are not caused by insufficient coverage as comparable read coverage is achieved (Figure 5D, left bottom panel). To validate the putative placenta-specific mgDMCs identified by CARSII, we analyzed the allelic DNA methylation using SNPs identified by CGmapTools (Guo et al., 2018). This analysis revealed 26 putative placenta-specific mgDMCs containing SNPs, and all of them showed significant allelic methylation (Figure S5D), validating the accuracy of CARSII in predicting mgDMCs within a single tissue. Next, we applied CARSII to monkey somatic tissue methylomes and identified an average of 61 putative mgDMCs, which is significantly fewer than the 146 identified in monkey placenta (Figure 5D, middle panel; Table S5), indicating mgDMCs are also enriched in monkey placenta. Interestingly, a similar analysis revealed that the placenta enrichment of mgDMCs is not observed in mice (Figure 5D, right panel), indicating that it is a primate-specific phenomenon.

Next, we examined whether PEG-emDMRs in human and monkey early embryos are biasedly maintained in placenta. Since the mgDMRs predicted by CARSII is restricted to CpG islands, our analysis of PEG-emDMR maintenance in placenta were only focused on the PEG-emDMRs that overlapped with emDMCs (PEG-emDMCs). We first identified 50 and 75 PEG-emDMCs in human and monkey early embryos, respectively (Figure S5E). 9 out of the 50 (18.0%) PEG-emDMCs in humans and 11 out of the 75 (14.6%) PEG-emDMCs in monkeys overlap

Figure 5. mgDMCs of primates are highly enriched in placenta compared with those in somatic tissues

(A and B) UCSC genome browser snapshots showing 5mC levels of human-placenta-specific mgDMRs (or their homologies in monkey) in uniparental embryos and somatic tissues of humans (A) and monkeys (*Macaca fascicularis*) (B) (upper panel). The bottom panels show percentages of the methylated reads versus total reads at the related germline DMRs in placenta.

(C) A schematic representation of CARSII. Briefly, emDMCs were identified by comparing parental-specific DNA methylation in gametes or early embryos (left panel). Then, emDMCs that enriched for both hypomethylated and hypermethylated reads are considered as candidate mgDMCs (middle panel). Finally, only candidates showing consistent methylation along CGIs were considered as putative mgDMCs.

(D) Bar graphs showing the number of putative mgDMCs identified by CARSII in placenta and somatic tissues of humans (left panel), monkeys (*Macaca fascicularis*, middle panel), and mice (right panel). The percentages of emDMCs that meet the requirement of qualified reads (number > 20) in each tissue are shown in the bottom panels.

See also Figure S5 and Tables S1, S4, and S5.

Please cite this article in press as: Chu et al., Analysis of developmental imprinting dynamics in primates using SNP-free methods to identify imprinting defects in cloned placenta, Developmental Cell (2021), https://doi.org/10.1016/j.devcel.2021.09.012

CellPress

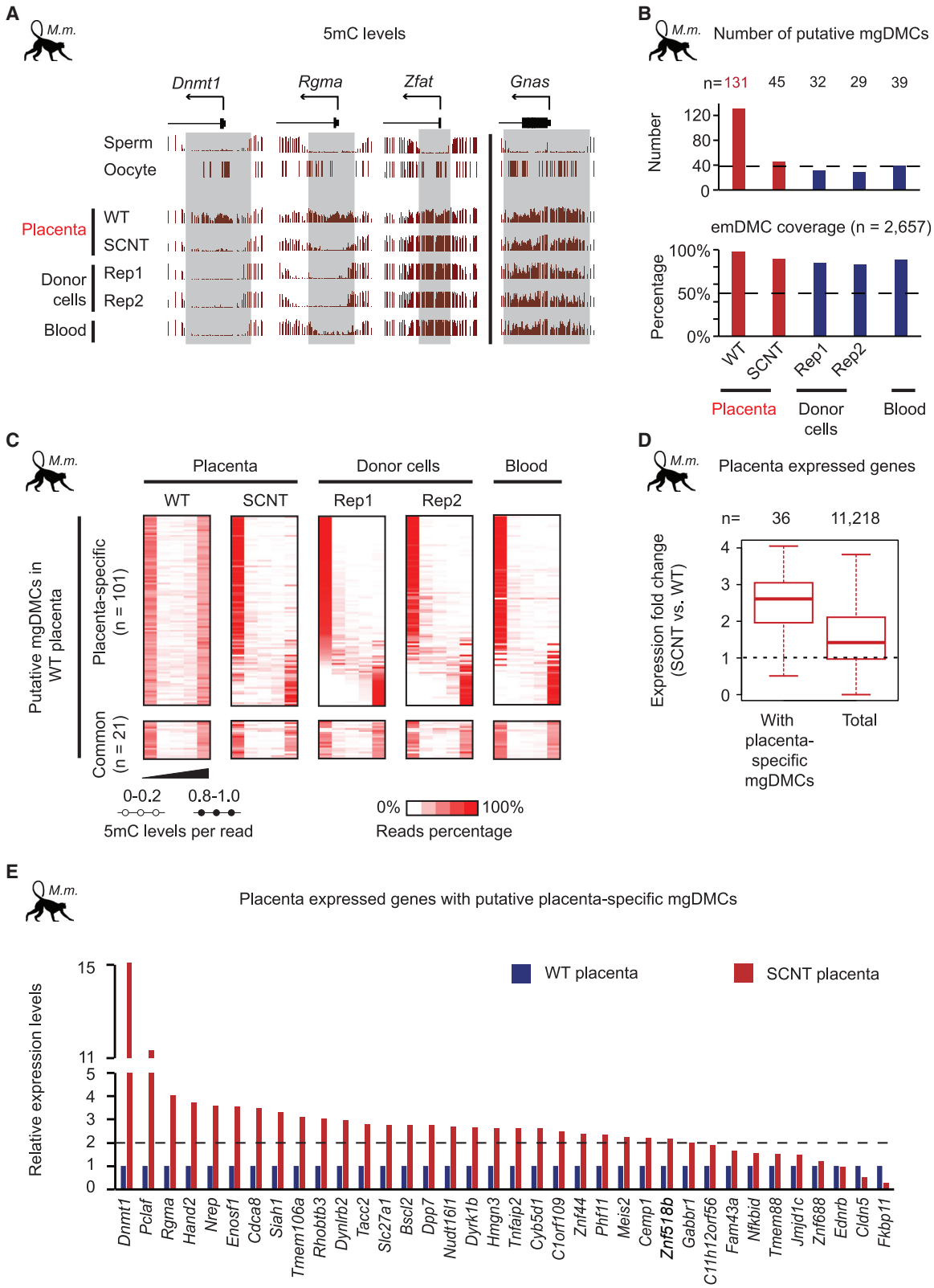

Figure 6. Global loss of placenta-specific mgDMCs in monkey SCNT placenta

(A) UCSC genome browser snapshots showing 5mC levels of monkey homologies of representative known human placenta-specific mgDMRs in different cells of monkeys (*Macaca mulatta*). *Gnas* is a common mgDMR in placenta and somatic tissues.

(legend continued on next page)

Please cite this article in press as: Chu et al., Analysis of developmental imprinting dynamics in primates using SNP-free methods to identify imprinting defects in cloned placenta, Developmental Cell (2021), https://doi.org/10.1016/j.devcel.2021.09.012

with the putative mgDMCs in placenta (Figure S5E), indicating PEGs in early embryos and placenta are also largely different. Taken together, our analyses revealed that the majority of the PEGs in early embryos have lost their imprinted state in both embryonic and extraembryonic-derived tissues. In addition, placenta of humans and monkeys, but not mice, has about three times as many mgDMCs as that in somatic tissues.

Global loss of placenta-specific mgDMCs in monkey SCNT placenta

The significant enrichment of mgDMCs in placenta compared with somatic tissues prompted us to ask whether the placenta-specific imprinting would be lost in monkey SCNT placenta, considering that donor cells (cumulus cells or fibroblast) are of embryonic, but not extraembryonic, origin (Liu et al., 2018). To this end, we profiled the placenta methylomes of newborn monkeys (*Macaca mulatta*) derived from both natural mating (WT) and SCNT using fibroblast as donor cells. We also analyzed the donor cell methylome generated in this study, as well as blood cell methylome from a public dataset (Table S1). The global methylation level of SCNT placenta is lower than that of the donor cells and blood cells but higher than that of WT placenta (Figure S6A), indicating a global alteration of DNA methylation in monkey SCNT placenta. An initial inspection of the monkey counterparts of known placenta-specific mgDMRs in humans revealed they become either hypomethylated or hypermethylated in SCNT placenta compared with that in WT placenta (Figures 5A, 6A, and S6B), indicating that their imprinted states are lost in monkey SCNT placenta. In contrast, the methylation pattern of mgDMRs (e.g., *Gnas* DMR), which does not exhibit a difference between placenta and somatic tissues, does not exhibit alteration in SCNT placenta compared with that in WT placenta (Figures 6A and S6B). These initial observations raised the possibility that loss of placenta-specific mgDMRs in monkey SCNT placenta might be caused by the different imprinted states between the donor fibroblast (embryonic origin) and the placenta (extraembryonic origin).

To determine whether loss of placenta-specific mgDMRs in monkey SCNT placenta happens genome-wide, we analyzed public monkey (*Macaca mulatta*) sperm and oocyte DNA methylome datasets (Gao et al., 2017) and identified 2,657 emDMCs (Figure S6C; Table S4). Based on these emDMCs, we then identified putative mgDMCs by CARSII in placenta, donor fibroblast cells, and blood cells of *Macaca mulatta* (Figure 6B; Table S5). Similar to the observations in humans and *Macaca fascicularis*, we found that putative mgDMCs are also enriched in placenta (n = 131) compared with that in fibroblast donor cells (n = 32 and 29), or blood cells (n = 39) of *Macaca mulatta* (Figure 6B). However, only 45 putative mgDMCs were identified in SCNT placenta, which is similar to those identified in donor cells or blood cells (Figure 6B). This result indicates that imprinting in monkey SCNT placenta is severely compromised. To analyze the methylation change of the 131 putative mgDMCs in detail, we separated them into placenta-specific mgDMCs (n = 101) and common mgDMCs (n = 21) (the others are unclear) (Figure 6C; Table S5). As expected, most of the placenta-specific mgDMCs have lost their imprinted states (bi-module distribution) to become either hypomethylated or hypermethylated state in SCNT placenta (Figure 6C). In contrast, the common mgDMCs still maintain their imprinted states (Figure 6C). Interestingly, the DNA methylation state of placenta-specific mgDMCs in SCNT placenta closely resembles that of the donor cells but not WT placenta (Figure 6C), indicating the loss of germline imprinting in somatic tissues cannot be regained through SCNT reprogramming. Taken together, our results demonstrate a global loss of placenta-specific mgDMCs in monkey SCNT placenta, which is likely due to the imprinting differences between the donor cells and the placenta in primates.

Placenta-specific imprinted genes are dysregulated in monkey SCNT placenta

To determine the transcriptional effect of losing placenta-specific mgDMCs in monkey SCNT placenta, we performed comparative transcriptome analysis in monkey WT and SCNT placenta. We focus the analysis on genes that express in placenta (FPKM $\geq$ 1) and have at least one putative placenta-specific mgDMC located in promoter (transcription start site ± 2.5 kb). Using these criteria, we identified 36 candidate genes that are associated with 34 putative placenta-specific mgDMCs. Notably, almost all these 34 putative placenta-specific mgDMCs exhibit loss of DNA methylation in SCNT placenta (Figure S6D), indicating the genes regulated by these putative mgDMCs have switched from mono-allelic expression to bi-allelic expression, resulting in increased gene expression. Consistently, we observed a median increase of 2.6-fold in their expression in SCNT placenta compared with that in WT placenta (Figures 6D and 6E). In contrast, the total placenta-expressed genes only have a median 1.4-fold increase (Figure 6D). Considering the fact that mgDMCs do not represent all mgDMRs in a certain tissue (Figure S5B) and the imprinting control regions can be located in distal regions outside promoters (Zink et al., 2018), it is expected that more imprinted genes than the ones we identified are dysregulated in monkey SCNT placenta.

DISCUSSION

TARSII and CARSII analyses have enabled us to identify germline DMRs in humans and monkeys without SNP information.

(B) A bar graph showing the number of putative mgDMCs identified by CARSII in different cells of monkeys (*Macaca mulatta*) (upper panels). The percentage of emDMCs meet the requirement of qualified reads (number > 20) in each tissue are shown in the bottom panels.
(C) Heatmaps showing the percentages of methylated reads versus total reads at putative mgDMCs in different cells of monkeys (*Macaca mulatta*). The placenta-specific and common mgDMCs were categorized and analyzed separately (Table S5).
(D) Boxplot showing fold changes of gene expression levels (FPKM) comparing WT and SCNT monkey placenta (SCNT versus WT). The placenta-expressed genes that have at least one putative placenta-specific mgDMC at promoter (left) were compared with all expressed genes in placenta (right).
(E) A bar graph showing relative gene expression levels (FPKM) comparing WT and SCNT monkey placenta (divided by gene FPKM of WT placenta) for the 36 genes related to Figure 6D.
See also Figure S6 and Tables S1, S4, and S5.

The analyses allowed us to make two major conclusions regarding developmental imprinting dynamics in primates. First, imprinting in early embryos and somatic tissues is different as most PEG-emDMRs in early embryos are not maintained as mgDMRs in somatic tissues or placenta (Figures 4B, 4C, and S5E). This is likely due to DNA methylation reprogramming during post-implantation development (Figures 4D and 4E). Second, compared with mice, primates exhibit greater difference in mgDMRs between embryonic-derived and extraembryonic-derived tissues (Figures 5D and 6B). Based on these observations, we propose a model to illustrate how the abundant mgDMRs in early embryos are reprogrammed in different tissues during primate embryonic development (Figure S6E). Based on this model, somatic tissues of primates preserve much fewer mgDMRs compared with early embryos or placenta (Figure S6E). Interestingly, such dememorization of mgDMRs is non-reversible and could lead to imprinting defects in placenta of developing embryos generated from somatic cell reprogramming (Figures 6 and S6E).

Our discovery of severe imprinting defects in cloned monkey placenta also revealed a major difference regarding the barriers of mouse and primate cloning. Although both mice and primates share the H3K9me3 reprogramming defects in early embryos that prevents ZGA (Chung et al., 2015; Liu et al., 2018; Matoba et al., 2014), the post-implantation barriers appear to be different. While defects in H3K27me3-dependent placenta-specific imprinting on *Sfmbt2*, *Gab1*, *Somc1*, and *Pfh17* were observed in mouse SCNT embryos (Matoba et al., 2018) and were recently confirmed as important barriers in mouse cloning (Inoue et al., 2020; Wang et al., 2020), similar defects are unlikely to exist in cloned monkeys as maternal H3K27me3 is not well maintained in monkey early embryos (Figures 2 and S2). Instead, we observed a much higher enrichment of placenta-specific mgDMRs in monkey placenta than that in mouse placenta (Figures 5D and 6B), indicating a much more severe loss of placenta-specific allelic DNA methylation and imprinted expression in cloned monkeys. Considering the importance of placenta-specific imprinted genes in mouse cloning (Inoue et al., 2020; Wang et al., 2020), the large imprinting defects in cloned monkey placenta likely contribute to the extremely low efficiency of monkey cloning.

In support of the above notion, at least some of the defective imprinted genes in cloned monkey placenta (Figure 6E) are involved in embryonic development. For examples, the expression level of *DNMT1* is positively correlated with human placenta growth (Mukhopadhyay et al., 2016). In mice, knocking out *Hand2* or its homolog *Hand1* resulted in embryonic lethality due to severe placenta defects (McFadden et al., 2005). In addition, *RHOBTB3*, *SIAH1*, and *TNFAIP2* play an important role in regulating cell proliferation (Adam et al., 2015; Jia et al., 2018; Lu and Pfeffer, 2013). Future work should investigate the functions of the placenta-specific imprinted genes in primate embryonic development and test whether restoring the allelic expression of functionally relevant imprinted genes in placenta will improve cloning efficiency. It is also interesting to test whether using extraembryonic donor cells for SCNT or performing tetraploid complementation can increase monkey cloning efficiency.

Limitation of the study

We would like to note that, while TARSII and CARSII are efficient in predicting germline DMRs in an SNP-independent manner, a low false-positive discoveries rate is noted. Thus, stringent confirmation of imprinting status at certain DMR requires SNP-based allelic analyses.

STAR★METHODS

Detailed methods are provided in the online version of this paper and include the following:

- KEY RESOURCES TABLE
- RESOURCE AVAILABILITY
  - Lead contact
  - Materials availability
  - Data and code availability
- EXPERIMENTAL MODEL AND SUBJECT DETAILS
  - Animal ethics statements
- METHOD DETAILS
  - Super-ovulation and oocyte collection
  - Intracytoplasmic sperm injection (ICSI)
  - Parthenogenetic (PG) embryo collection
  - Androgenetic (AG) embryo collection
  - Monkey SCNT
  - Embryo immunofluorescent staining
  - Transcriptome profiling in monkey early embryos
  - H3K27me3 profiling in monkey early embryos
  - Post-bisulfite adaptor tagging (PBAT)
  - Whole genome bisulfite sequencing profiling (WGBS)
  - Transcriptome profiling in monkey placenta
- QUANTIFICATION AND STATISTICAL ANALYSIS
  - Data mapping and processing
  - RNA-seq processing
  - CUT&RUN
  - PBAT and WGBS
  - Identification of paternal-biased expressed genes (PEGs)
  - Identification of maternal-allele-methylated differentially methylated regions (mDMRs)
  - Identification of ZGA genes in *Macaca fascicularis*
  - Global correlation analysis of H3K27me3
  - Identification of AG and PG-biased H3K27me3 regions
  - Identification of putative imprinted DMRs by TARSII
  - Identification of putative maternal germline DMCs by CARSII
  - Calculation of false positive rates (FPRs) of mDMCs identified by CARSII in certain methylome
  - Allelic DNA methylation analysis

SUPPLEMENTAL INFORMATION

Supplemental information can be found online at https://doi.org/10.1016/j.devcel.2021.09.012.

ACKNOWLEDGMENTS

We thank members of the Zhang lab Drs. Zhiyuan Chen, Chunxia Zhang, Meng Wang, and Yisi Li for helpful discussion and comments on the manuscript and members of the Yunnan Key Laboratory of Primate Biomedical Research

facility for excellent animal welfare and husbandry. This work is supported by funding from the Howard Hughes Medical Institute (to Y.Z.), the National Key Research and Development Program (2018YFA0801403, 2016YFA0101401) (to Y.N.), and Major Basic Research Project of Science and Technology of Yunnan (202001BC07001) (to W.J.); Y.Z. is an investigator of the Howard Hughes Medical Institute.

AUTHOR CONTRIBUTIONS

Y.Z. and W.J. conceived the project; Y.Z. supervised the work by W.Z.; W.Z. developed the SNP-free TARSII and CARSII methods and performed all the data analysis; Y.N. and W.J. supervised the work by C.C., Y.K., and C.S.; Y.K. and C.C. performed the monkey embryo and SCNT experiments and collected the samples; W.Z. taught C.C. for library preparation, and both W.Z. and C.C. prepared the libraries; C.S. performed H3K27me3 immunofluorescent staining; Y.Z. and W.Z. organized and wrote the manuscript.

DECLARATION OF INTERESTS

The authors declare no competing interests.

Received: June 12, 2021
Revised: August 25, 2021
Accepted: September 10, 2021
Published: October 6, 2021

REFERENCES

Adam, M.G., Matt, S., Christian, S., Hess-Stumpp, H., Haegebarth, A., Hofmann, T.G., and Algire, C. (2015). SIAH ubiquitin ligases regulate breast cancer cell migration and invasion independent of the oxygen status. Cell Cycle *14*, 3734–3747.

Babak, T., DeVeale, B., Tsang, E.K., Zhou, Y., Li, X., Smith, K.S., Kukurba, K.R., Zhang, R., Li, J.B., van der Kooy, D., et al. (2015). Genetic conflict reflected in tissue-specific maps of genomic imprinting in human and mouse. Nat. Genet. *47*, 544–549.

Barlow, D.P., and Bartolomei, M.S. (2014). Genomic imprinting in mammals. Cold Spring Harb. Perspect. Biol. *6*, a018382.

Cao, R., Wang, L., Wang, H., Xia, L., Erdjument-Bromage, H., Tempst, P., Jones, R.S., and Zhang, Y. (2002). Role of histone H3 lysine 27 methylation in Polycomb-group silencing. Science *298*, 1039–1043.

Chan, A.W., and Yang, S.H. (2009). Generation of transgenic monkeys with human inherited genetic disease. Methods *49*, 78–84.

Chen, Y., Niu, Y., Yang, S., He, X., Ji, S., Si, W., Tang, X., Xie, Y., Wang, H., Lu, Y., et al. (2012). The available time window for embryo transfer in the rhesus monkey (Macaca mulatta). Am. J. Primatol. *74*, 165–173.

Chen, Z., Yin, Q., Inoue, A., Zhang, C., and Zhang, Y. (2019). Allelic H3K27me3 to allelic DNA methylation switch maintains noncanonical imprinting in extraembryonic cells. Sci. Adv. *5*, eaay7246.

Chen, Z., and Zhang, Y. (2020). Maternal H3K27me3-dependent autosomal and X chromosome imprinting. Nat. Rev. Genet. *21*, 555–571.

Cheong, C.Y., Chng, K., Ng, S., Chew, S.B., Chan, L., and Ferguson-Smith, A.C. (2015). Germline and somatic imprinting in the nonhuman primate highlights species differences in oocyte methylation. Genome Res *25*, 611–623.

Chung, Y.G., Matoba, S., Liu, Y., Eum, J.H., Lu, F., Jiang, W., Lee, J.E., Sepilian, V., Cha, K.Y., Lee, D.R., and Zhang, Y. (2015). Histone demethylase expression enhances human somatic cell nuclear transfer efficiency and promotes derivation of pluripotent stem cells. Cell Stem Cell *17*, 758–766.

Court, F., Tayama, C., Romanelli, V., Martin-Trujillo, A., Iglesias-Platas, I., Okamura, K., Sugahara, N., Simón, C., Moore, H., Harness, J.V., et al. (2014). Genome-wide parent-of-origin DNA methylation analysis reveals the intricacies of human imprinting and suggests a germline methylation-independent mechanism of establishment. Genome Res *24*, 554–569.

de Sa Machado, A., da Silva, G., Francisco Junior, R., Dos Santos Ferreira, C., Mozer Rodrigues, P.T., Terra Machado, D., Louvain de Souza, T., Teixeira de Souza, J., Figueiredo Osorio da Silva, C., Alves da Silva, A.F., Andrade, C.C.F., et al. (2018). Maternal 5^{m}CpG Imprints at the *PARD6G-AS1* and *GCSAML* differentially methylated regions are decoupled from parent-of-origin expression effects in multiple human tissues. Front. Genet. *9*, 36.

Deaton, A.M., and Bird, A. (2011). CpG islands and the regulation of transcription. Genes Dev *25*, 1010–1022.

Gao, F., Niu, Y., Sun, Y.E., Lu, H., Chen, Y., Li, S., Kang, Y., Luo, Y., Si, C., Yu, J., et al. (2017). De novo DNA methylation during monkey pre-implantation embryogenesis. Cell Res *27*, 526–539.

Grothaus, K., Kanber, D., Gellhaus, A., Mikat, B., Kolarova, J., Siebert, R., Wieczorek, D., and Horsthemke, B. (2016). Genome-wide methylation analysis of retrocopy-associated CpG islands and their genomic environment. Epigenetics *11*, 216–226.

Guo, W., Zhu, P., Pellegrini, M., Zhang, M.Q., Wang, X., and Ni, Z. (2018). CGmapTools improves the precision of heterozygous SNV calls and supports allele-specific methylation detection and visualization in bisulfite-sequencing data. Bioinformatics *34*, 381–387.

Hamada, H., Okae, H., Toh, H., Chiba, H., Hiura, H., Shirane, K., Sato, T., Suyama, M., Yaegashi, N., Sasaki, H., and Arima, T. (2016). Allele-specific methylome and transcriptome analysis reveals widespread imprinting in the human placenta. Am. J. Hum. Genet. *99*, 1045–1058.

Hanna, C.W., Peñaherrera, M.S., Saadeh, H., Andrews, S., McFadden, D.E., Kelsey, G., and Robinson, W.P. (2016). Pervasive polymorphic imprinted methylation in the human placenta. Genome Res *26*, 756–767.

Inoue, A., Jiang, L., Lu, F., Suzuki, T., and Zhang, Y. (2017). Maternal H3K27me3 controls DNA methylation-independent imprinting. Nature *547*, 419–424.

Inoue, K., Ogonuki, N., Kamimura, S., Inoue, H., Matoba, S., Hirose, M., Honda, A., Miura, K., Hada, M., Hasegawa, A., et al. (2020). Loss of H3K27me3 imprinting in the Sfmbt2 miRNA cluster causes enlargement of cloned mouse placentas. Nat. Commun. *11*, 2150.

Jadhav, B., Monajemi, R., Gagalova, K.K., Ho, D., Draisma, H.H.M., van de Wiel, M.A., Franke, L., Heijmans, B.T., van Meurs, J., Jansen, R., et al. (2019). RNA-Seq in 296 phased trios provides a high-resolution map of genomic imprinting. BMC Biol *17*, 50.

Jia, L., Shi, Y., Wen, Y., Li, W., Feng, J., and Chen, C. (2018). The roles of TNFAIP2 in cancers and infectious diseases. J. Cell. Mol. Med. *22*, 5188–5195.

Joshi, R.S., Garg, P., Zaitlen, N., Lappalainen, T., Watson, C.T., Azam, N., Ho, D., Li, X., Antonarakis, S.E., Brunner, H.G., et al. (2016). DNA methylation profiling of uniparental disomy subjects provides a map of parental epigenetic bias in the human genome. Am. J. Hum. Genet. *99*, 555–566.

Kikyo, N., Williamson, C.M., John, R.M., Barton, S.C., Beechey, C.V., Ball, S.T., Cattanach, B.M., Surani, M.A., and Peters, J. (1997). Genetic and functional analysis of neuronatin in mice with maternal or paternal duplication of distal Chr 2. Dev. Biol. *190*, 66–77.

Kim, D., Pertea, G., Trapnell, C., Pimentel, H., Kelley, R., and Salzberg, S.L. (2013). TopHat2: accurate alignment of transcriptomes in the presence of insertions, deletions and gene fusions. Genome Biol *14*, R36.

Krueger, F., and Andrews, S.R. (2011). Bismark: a flexible aligner and methylation caller for bisulfite-Seq applications. Bioinformatics *27*, 1571–1572.

Langmead, B., and Salzberg, S.L. (2012). Fast gapped-read alignment with Bowtie 2. Nat. Methods *9*, 357–359.

Leng, L., Sun, J., Huang, J., Gong, F., Yang, L., Zhang, S., Yuan, X., Fang, F., Xu, X., Luo, Y., et al. (2019). Single-cell transcriptome analysis of uniparental embryos reveals parent-of-origin effects on human preimplantation development. Cell Stem Cell *25*, 697–712.e6.

Liu, Z., Cai, Y., Wang, Y., Nie, Y., Zhang, C., Xu, Y., Zhang, X., Lu, Y., Wang, Z., Poo, M., and Sun, Q. (2018). Cloning of macaque monkeys by somatic cell nuclear transfer. Cell *172*, 881–e887.e7.

Liu, Z., Nie, Y.H., Zhang, C.C., Cai, Y.J., Wang, Y., Lu, H.P., Li, Y.Z., Cheng, C., Qiu, Z.L., and Sun, Q. (2016). Generation of macaques with sperm derived from juvenile monkey testicular xenografts. Cell Res *26*, 139–142.

Lu, A., and Pfeffer, S.R. (2013). Golgi-associated RhoBTB3 targets cyclin E for ubiquitylation and promotes cell cycle progression. J. Cell Biol. *203*, 233–250.

Matoba, S., Liu, Y., Lu, F., Iwabuchi, K.A., Shen, L., Inoue, A., and Zhang, Y. (2014). Embryonic development following somatic cell nuclear transfer impeded by persisting histone methylation. Cell *159*, 884–895.

Matoba, S., Wang, H., Jiang, L., Lu, F., Iwabuchi, K.A., Wu, X., Inoue, K., Yang, L., Press, W., Lee, J.T., et al. (2018). Loss of H3K27me3 imprinting in somatic cell nuclear transfer embryos disrupts post-implantation development. Cell Stem Cell *23*, 343–354.e5.

McFadden, D.G., Barbosa, A.C., Richardson, J.A., Schneider, M.D., Srivastava, D., and Olson, E.N. (2005). The Hand1 and Hand2 transcription factors regulate expansion of the embryonic cardiac ventricles in a gene dosage-dependent manner. Development *132*, 189–201.

Miura, F., Enomoto, Y., Dairiki, R., and Ito, T. (2012). Amplification-free whole-genome bisulfite sequencing by post-bisulfite adaptor tagging. Nucleic Acids Res *40*, e136.

Mukhopadhyay, A., Ravikumar, G., Meraaj, H., Dwarkanath, P., Thomas, A., Crasta, J., Thomas, T., Kurpad, A.V., and Sridhar, T.S. (2016). Placental expression of DNA methyltransferase 1 (DNMT1): gender-specific relation with human placental growth. Placenta *48*, 119–125.

Niu, Y., Yu, Y., Bernat, A., Yang, S., He, X., Guo, X., Chen, D., Chen, Y., Ji, S., Si, W., et al. (2010). Transgenic rhesus monkeys produced by gene transfer into early-cleavage-stage embryos using a simian immunodeficiency virus-based vector. Proc. Natl. Acad. Sci. USA *107*, 17663–17667.

Peters, J. (2014). The role of genomic imprinting in biology and disease: an expanding view. Nat. Rev. Genet. *15*, 517–530.

Picelli, S., Björklund, Å.K., Faridani, O.R., Sagasser, S., Winberg, G., and Sandberg, R. (2013). Smart-seq2 for sensitive full-length transcriptome profiling in single cells. Nat. Methods *10*, 1096–1098.

Proudhon, C., Duffié, R., Ajjan, S., Cowley, M., Iranzo, J., Carbajosa, G., Saadeh, H., Holland, M.L., Oakey, R.J., Rakyan, V.K., et al. (2012). Protection against de novo methylation is instrumental in maintaining parent-of-origin methylation inherited from the gametes. Mol. Cell *47*, 909–920.

Rueden, C.T., Schindelin, J., Hiner, M.C., DeZonia, B.E., Walter, A.E., Arena, E.T., and Eliceiri, K.W. (2017). ImageJ2: ImageJ for the next generation of scientific image data. BMC Bioinformatics *18*, 529.

Sagi, I., De Pinho, J.C., Zuccaro, M.V., Atzmon, C., Golan-Lev, T., Yanuka, O., Prosser, R., Sadowy, A., Perez, G., Cabral, T., et al. (2019). Distinct imprinting signatures and biased differentiation of human androgenetic and parthenogenetic embryonic stem cells. Cell Stem Cell *25*, 419–432.e9.

Sanchez-Delgado, M., Court, F., Vidal, E., Medrano, J., Monteagudo-Sánchez, A., Martin-Trujillo, A., Tayama, C., Iglesias-Platas, I., Kondova, I., Bontrop, R., et al. (2016). Human oocyte-derived methylation differences persist in the placenta revealing widespread transient imprinting. PLoS Genet *12*, e1006427.

Skene, P.J., and Henikoff, S. (2017). An efficient targeted nuclease strategy for high-resolution mapping of DNA binding sites. eLife *6*, e21856.

Smallwood, S.A., Tomizawa, S., Krueger, F., Ruf, N., Carli, N., Segonds-Pichon, A., Sato, S., Hata, K., Andrews, S.R., and Kelsey, G. (2011). Dynamic CpG island methylation landscape in oocytes and preimplantation embryos. Nat. Genet. *43*, 811–814.

Trapnell, C., Roberts, A., Goff, L., Pertea, G., Kim, D., Kelley, D.R., Pimentel, H., Salzberg, S.L., Rinn, J.L., and Pachter, L. (2012). Differential gene and transcript expression analysis of RNA-seq experiments with TopHat and Cufflinks. Nat. Protoc. *7*, 562–578.

Tucci, V., Isles, A.R., Kelsey, G., and Ferguson-Smith, A.C.; Erice Imprinting Group (2019). Genomic imprinting and physiological processes in mammals. Cell *176*, 952–965.

Wang, L.-Y., Li, Z.-K., Wang, L.-B., Liu, C., Sun, X.-H., Feng, G.-H., Wang, J.-Q., Li, Y.-F., Qiao, L.-Y., Nie, H., et al. (2020). Overcoming intrinsic H3K27me3 imprinting barriers improves post-implantation development after somatic cell nuclear transfer. Cell Stem Cell *27*, 315–325.e5.

Wei, Q., Sun, Z., He, X., Tan, T., Lu, B., Guo, X., Su, B., and Ji, W. (2011). Derivation of rhesus monkey parthenogenetic embryonic stem cells and its microRNA signature. PLoS One *6*, e25052.

Wianny, F., Blachère, T., Godet, M., Guillermas, R., Cortay, V., Bourillot, P.Y., Lefèvre, A., Savatier, P., and Dehay, C. (2016). Epigenetic status of H19/IGF2 and SNRPN imprinted genes in aborted and successfully derived embryonic stem cell lines in non-human primates. Stem Cell Res *16*, 557–567.

Xia, W., Xu, J., Yu, G., Yao, G., Xu, K., Ma, X., Zhang, N., Liu, B., Li, T., Lin, Z., et al. (2019). Resetting histone modifications during human parental-to-zygotic transition. Science *365*, 353–360.

Xie, W., Barr, C.L., Kim, A., Yue, F., Lee, A.Y., Eubanks, J., Dempster, E.L., and Ren, B. (2012). Base-resolution analyses of sequence and parent-of-origin dependent DNA methylation in the mouse genome. Cell *148*, 816–831.

Yang, H., Shi, L., Wang, B.A., Liang, D., Zhong, C., Liu, W., Nie, Y., Liu, J., Zhao, J., Gao, X., et al. (2012). Generation of genetically modified mice by oocyte injection of androgenetic haploid embryonic stem cells. Cell *149*, 605–617.

Zhang, W., Chen, Z., Yin, Q., Zhang, D., Racowsky, C., and Zhang, Y. (2019). Maternal-biased H3K27me3 correlates with paternal-specific gene expression in the human morula. Genes Dev *33*, 382–387.

Zheng, H., Huang, B., Zhang, B., Xiang, Y., Du, Z., Xu, Q., Li, Y., Wang, Q., Ma, J., Peng, X., et al. (2016). Resetting epigenetic memory by reprogramming of histone modifications in mammals. Mol. Cell *63*, 1066–1079.

Zhu, P., Guo, H., Ren, Y., Hou, Y., Dong, J., Li, R., Lian, Y., Fan, X., Hu, B., Gao, Y., et al. (2018). Single-cell DNA methylome sequencing of human preimplantation embryos. Nat. Genet. *50*, 12–19.

Zink, F., Magnusdottir, D.N., Magnusson, O.T., Walker, N.J., Morris, T.J., Sigurdsson, A., Halldorsson, G.H., Gudjonsson, S.A., Melsted, P., Ingimundardottir, H., et al. (2018). Insights into imprinting from parent-of-origin phased methylomes and transcriptomes. Nat. Genet. *50*, 1542–1552.